


High-gradient rf tests of welded X-band accelerating cavitiesV. A. Dolgashev,^{1,*} L. Faillace², B. Spataro³, S. Tantawi,¹ and R. Bonifazi³¹SLAC National Accelerator Laboratory, Menlo Park, California 94025, USA²INFN–Laboratori Nazionali di Frascati, Via E. Fermi 40, Frascati (Roma) 00044, Italy³Comeb srl, Via dei Ranuncoli snc, Roma 00134, Italy (Received 4 June 2020; revised 4 May 2021; accepted 16 July 2021; published 10 August 2021)

Linacs for high-energy physics, as well as for industry and medicine, require accelerating structures which are compact, robust, and cost-effective. Small foot-print linacs require high-accelerating gradients. Currently, stable-operating gradients, exceeding 100 MV/m, have been demonstrated at SLAC National Accelerator Laboratory, CERN, and KEK at X-band frequencies. Recent experiments show that accelerating cavities made out of hard copper alloys achieve better high-gradient performance as compared with soft copper cavities. In the scope of a decade-long collaboration between SLAC, INFN-Frascati, and KEK on the development of innovative high-gradient structures, this particular study focuses on the technological developments directed to show the viability of novel welding techniques. Two novel X-band accelerating structures, made out of hard copper, were fabricated at INFN-Frascati by means of clamping and welding. One cavity was welded with the electron beam and the other one with the tungsten inert gas welding process. In the technological development of the construction methods of high-gradient accelerating structures, high-power testing is a critical step for the verification of their viability. Here, we present the outcome of this step—the results of the high-power rf tests of these two structures. These tests include the measurements of the breakdown rate probability used to characterize the behavior of vacuum rf breakdowns, one of the major factors limiting the operating accelerating gradients. The electron beam welded structure demonstrated accelerating gradients of 90 MV/m at a breakdown rate of 10^{-3} /(pulse meter) using a shaped pulse with a 150 ns flat part. Nevertheless, it did not achieve its ultimate performance because of arcing in the mode launcher power coupler. On the other hand, the tungsten inert gas welded structure reached its ultimate performance and operated at about a 150 MV/m gradient at a breakdown rate of 10^{-3} /(pulse meter) using a shaped pulse with a 150 ns flat part. The results of both experiments show that welding, a robust, and low-cost alternative to brazing or diffusion bonding, is viable for high-gradient operation. This approach enables the construction of multicell standing and traveling-wave accelerating structures.

DOI: [10.1103/PhysRevAccelBeams.24.081002](https://doi.org/10.1103/PhysRevAccelBeams.24.081002)**I. INTRODUCTION**

There is a strong demand for accelerating structures that are able to achieve higher gradients for the next generation of linear particle accelerators for research, industrial, and medical applications.

A continuous collaboration on the study of various geometries, materials, surface processing techniques, and technological developments of accelerating structures has involved, for more than a decade, the SLAC National Accelerator Laboratory in the USA, the Italian Institute of Nuclear Physics–National Laboratories of Frascati (INFN-

LNF), and the High Energy Accelerator Research Organization (KEK) in Japan. The results of this study can be found in Refs. [1–23]. This paper is part of this study and in particular it focuses on the technological developments directed to show the viability of novel welding techniques [2–4,12].

The accelerating gradient is one of the major parameters that determines the cost and viability of accelerator projects, such as large-scale linear colliders for high-energy physics and high-brightness electron sources of free-electron lasers, for example, the Eupraxia@SparcLAB [24] and SLAC Linac Coherent Light Source [25].

The major issues determining the high-gradient performance of accelerating structures are the vacuum rf breakdown, pulse surface heating, and field emission. The rf breakdown abruptly and significantly changes the transmission and reflection of the rf power that is being coupled into an accelerating structure [1]. The rf breakdown physics is an active field and the main method of studying it is

*dolgash@slac.stanford.edu

Published by the American Physical Society under the terms of the *Creative Commons Attribution 4.0 International license*. Further distribution of this work must maintain attribution to the author(s) and the published article's title, journal citation, and DOI.

experimental, where we typically report the breakdown probability, i.e., the number of breakdowns per total number of rf pulses per meter at a given accelerating gradient and pulse shape. Numerous theoretical predictions and experiments have been carried out in the major national laboratories in order to evaluate the high-gradient performance of accelerating structures made out of different materials and operating at different frequencies [26–34].

Now, X-band structures are the most studied in terms of rf breakdowns [5–8,10,35–37]. A major part of this study is the technological activities, which resulted in the development of sophisticated manufacturing, surface preparation techniques, and systematic rf processing methods [21,22,38]. We know that breakdown statistics depend on pulse surface heating [9] and a numerous other factors, such as the peak electric field, the peak magnetic field [11], the peak Poynting vector [39], the hardness of the cavity material [12], and the cavity temperature [15,16].

For these systematic breakdown studies using high-gradient experiments, we developed three-cell cavities [7,12]. In these cavities, only the central cell’s electric and magnetic fields mimic the fields of a periodic full-scale standing-wave structure. We refer to these types of cavities as “single cell” because the field is highest only in the middle cell, while the first and third cells have lower fields. The peak on-axis electric field in the middle cell is two times higher than in the end-cells for the purpose of localizing rf breakdowns mostly in the middle cell. This geometry was developed specifically to test the basic physics of rf breakdowns. The test utilizes an economic setup with a reusable TM_{01} mode launcher power coupler [17,40]. With this configuration, we have tested more than 40 structures to date. As a result, a large amount of experimental data were produced and used here as a reference [5–14,17–20,23]. In these experiments, we tested structures fabricated with novel manufacturing techniques, including cavities built out of hard copper alloys. Our previous tests have demonstrated that structures made out of these hard copper alloys can achieve reliable accelerating gradients higher than 150 MV/m with rf breakdown rates better than that of soft annealed copper.

Commonly used methods for joining parts of accelerating structures are high-temperature brazing and diffusion bonding, which are performed at temperatures of 800–1000 °C. This high temperature anneals the metal and makes it soft. Although brazed cavities have good electrical, thermal, and vacuum properties, experimental results with hard copper cavities have shown that hard materials sustain higher accelerating gradients for the same breakdown rate, with the copper-silver (CuAg) alloy having the best performance. High-power tests of hard CuAg structures show gradients up to 200 MV/m at $10^{-3}/(\text{pulse meter})$ breakdown probability using a shaped pulse with a 150 ns flat part. Complementary to rf breakdown tests, studies of rf-induced pulse surface heating have shown that hard, non-annealed alloys such as

CuAg, CuCr, and CuZr exhibited significantly less damage than annealed copper [12–14].

These previous experiments [12–14], which have shown superior performance of the hard copper alloys in terms of higher accelerating gradients, were conducted in a setup which is unsuitable for practical applications, such as industrial or medical. This paper is directed to find a joining technique which allows for practical use of these alloys. The study of these alloys and compatible surface processing techniques will be part of further developments of high-gradient welded structures.

Since traditional high-temperature bonding makes copper soft, there is a need for practical processes that preserve the hardness of the material. The full study of building practical structures made of hard materials includes several developments, such as joining techniques, surface processing compatible with these techniques, and corresponding materials. This complete study is outside scope of this paper, which is specifically directed to the first step of this process—viability of novel joining techniques.

In this paper, we present the design and the high-power rf tests of two innovative single-cell accelerating X-band cavities that were manufactured without the high-temperature bonding process using cost-effective methods. The method of construction of these two prototypes, made out of hard copper, was published in Ref. [3]. We used two different processes for the vacuum sealing of the structures—electron beam welding (EBW) and tungsten Inert Gas (TIG) welding. These methods can be used to build practical multicell X-band cavities. Both the EBW and TIG processes assure a good vacuum envelope and robust mechanical assembly. For the weldings to be compatible with building high-gradient structures, several issues have to be resolved such as heating, deformations, and contamination of high-field surfaces.

For both the TIG and EBW structures, we have developed technological processes that dealt with these issues in order to preserve the cavity dimensions as well as its cleanliness [3]. During the electron beam welding, the heat generated by the electron beam is localized at the melting regions, therefore, not overheating the rest of the structure. In addition, the debris generated during melting of the joints stays confined in the secondary vacuum envelope [3]. As a result, the cleanliness of high-gradient surfaces of the cavity is preserved.

While TIG welding heats the structure more than EBW, it is a cheaper and simpler process. However, special care is needed in order to avoid overheating and contamination of the high-gradient surfaces.

The two prototypes were fabricated and low power tested at INFN, and then were shipped to SLAC for the high-power rf tests. Here, we will report the high-gradient performances of both prototypes.

First, we conducted experiments with the EBW cavity. During the test, we found that the cavity’s performance was

limited by arcing in the TM_{01} mode launcher to gradient levels lower than anticipated from our previous experience. As this limitation was understood, the waveguide system was reprocessed and the issue was solved. After that, we tested the TIG cavity, which reached its ultimate performance.

The EBW structure demonstrated an accelerating gradient of 90 MV/m at a breakdown rate of 10^{-3} /(pulse meter) using a shaped pulse with a 150 ns flat part. On the other hand, the TIG welded structure showed higher gradients of about 150 MV/m at the same breakdown rate and pulse shape.

We conjecture that, with further development, welded structures of this type can be used as practical accelerators by adding more cells and couplers [41]. This work maybe followed by systematic studies of material and compatible surface processing.

Moreover, the proposed EBW and TIG welded cavities are suitable for cryogenic operation and therefore can be run at even higher gradients [15,16]. At the end, a similar construction technique could be employed to build mm-wave accelerating structures [42,43].

II. CAVITY DESIGN AND CONSTRUCTION

In Fig. 1, we show the solid model of the clamped and then welded 11.4 GHz single-cell accelerating structure. This cavity construction is described in details in Ref. [3]. The main features of our clamping system are special screws [(2) in Fig. 1]. Thanks to this innovative approach, it is possible to obtain perfect rf contacts between the cells and the desired quality factor without using high-temperature bonding.

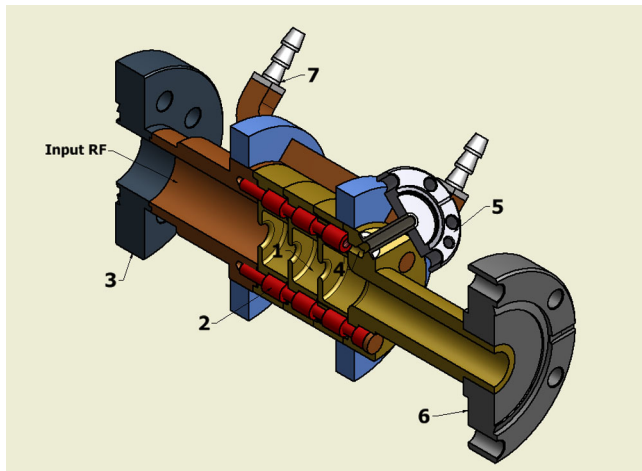


FIG. 1. Solid model, one-half of the welded single-cell cavity: (1) middle high-gradient cell, rf vacuum chamber, (2) special screws for clamping, (3) input rf flange, (4) secondary vacuum chamber, (5) Conflat vacuum flange for the secondary vacuum chamber, (6) downstream Conflat vacuum flange, and (7) water cooling pipe.

Two vacuum chambers are present in the structure. The primary rf vacuum chamber (1) is the volume inside the high-gradient accelerating cells where the rf power builds up the electromagnetic field. This chamber is connected to a vacuum pump through the input circular rf flange and the circular downstream vacuum flange [(3) and (6) in Fig. 1]. The secondary vacuum chamber (4) serves two important purposes: (1) it prevents virtual leaks (air pockets created between cells clamped together) from leaking gas into the primary vacuum chamber and (2) it reduces the risk of contamination of the primary chamber caused by the welding procedure performed on the outer surfaces of the cavity. We have derived the secondary vacuum approach from our previous multiple successful tests of clamped structures [1,2,6–14], where cells have a knife edge allowing for good rf contact. We consider this to be a robust approach at this stage of development. It is possible that, in the future, we may abandon the secondary vacuum if we will find it excessive.

The rf simulations of the cavity were carried out with Ansys High Frequency Simulation Software (HFSS) [44]. The electric and magnetic fields on the cavity mid-plane are shown in Fig. 2. These fields are normalized to a 100 MV/m accelerating gradient in the middle cell.

The geometry of the high-gradient middle cell is based on the geometry of a periodic accelerator structure cell. The main rf parameters for this cell are listed in Table I. In this table, Z_0 is 377 Ω , a is the iris aperture, $\lambda = 26.242$ mm is the free space wavelength at 11.424 GHz, and t is the iris thickness. All the field-dependent parameters are normalized to a 100 MV/m accelerating gradient for the speed of light particle. The rf power is coupled into the single-cell cavity by a circular waveguide using a TM_{01} mode launcher [17]. The central cell has an on-axis peak-field that is two times higher than that in the adjacent ones. The electromagnetic field inside the structure is excited at π mode. With this layout, breakdowns occur predominantly in the middle cell.

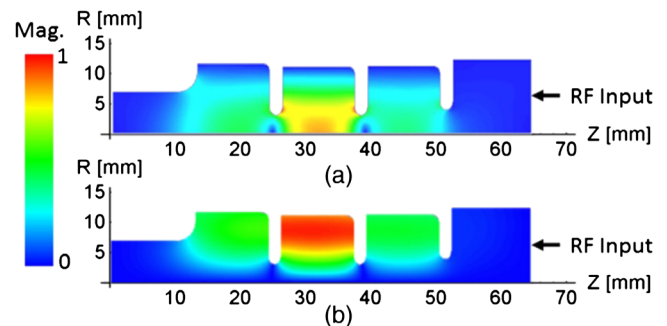


FIG. 2. Electric and magnetic fields on the cavity mid-plane which are scaled to a 100 MV/m accelerating gradient in the middle cell; (a) shows the mid-plane electric field, with a maximum of 202.9 MV/m and (b) shows the mid-plane magnetic field, with a maximum of 325 kA/m.

TABLE I. The parameters of the periodic structure normalized to a 100 MV/m accelerating gradient.

Parameter	Value
Resonant frequency, f [GHz]	11.424
Stored energy [J]	0.153
Quality factor Q	8590
Shunt impedance [M Ω /m]	102.894
H_{\max} [MA/m]	0.29
E_{\max} [MV/m]	203.1
Power loss per cell [MW]	1.275
a [mm]	2.75
a/λ	0.105
$H_{\max} Z_0/E_{\text{acc}}$	1.093
t [mm]	2
Iris ellipticity	1.385
Phase advance per cell (deg)	180

In Fig. 3, we show the EBW and TIG prototypes after welding. Since we tested a large number of cavities, we developed a comprehensive naming approach for them. These two particular structures are named “1C-SW-A2.75-T2.0-EBW-Cu-Frascati-#1” and “1C-SW-A2.75-T2.0-TIG-Cu-Frascati-#1” for the EBW and TIG, respectively. Here, “1C” indicates one high-gradient cell (the middle one), “SW” stands for standing-wave, “A” is the iris radius $a = 2.75$ mm, “T” is the iris wall thickness $t = 2$ mm, “EBW” and “TIG” are the processes used for the joining of the cells, “Cu” is copper, and “Frascati-#1” indicates that these are the first cavities of each type built at INFN-Frascati. The machining of both structures and the TIG welding was performed at Comeb srl [45], while the EBW

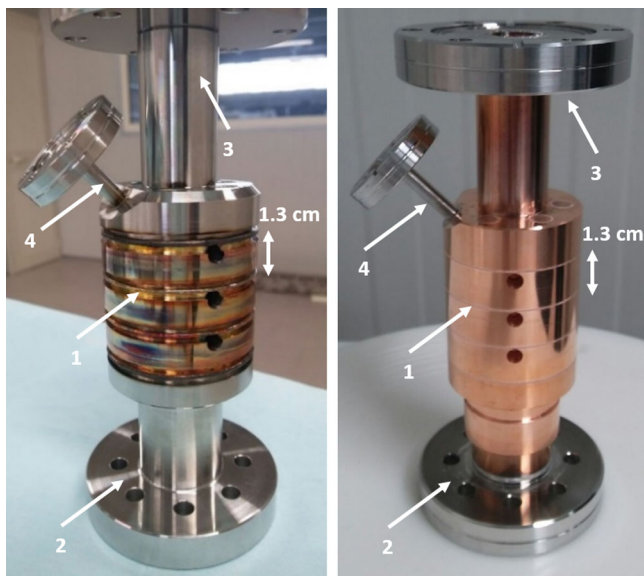


FIG. 3. Left, single-cell cavity after TIG welding. Right, single-cell cavity after EBW. (1) Welding joints, (2) input rf flange, (3) downstream Conflat vacuum flange, and (4) Conflat flange for pumping the secondary vacuum chamber.

was outsourced. The primary vacuum envelopes in both structures are geometrically identical. Each cell in the cavity is connected to the other by stainless steel screws that hold them tightly together. In order to accommodate the two different types of welding, the outside shape of the cell joints is different. The welding joints for the EBW and TIG are shown in Fig. 3.

III. LOW-POWER RF MEASUREMENTS

Before the welding of both prototypes, the initial rf characterization of the cavities was performed at INFN-LNF. The measured resonant frequency of the operating π mode corrected to vacuum was 11.4193 GHz for the TIG cavity and 11.4190 GHz for the EBW cavity. These structures were well within SLAC klystron bandwidth. After the two cavities were welded, they were shipped to

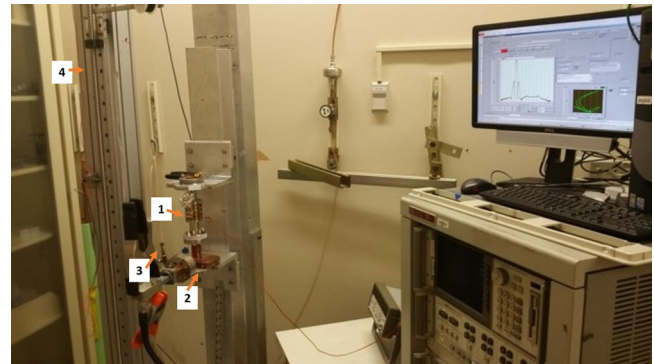


FIG. 4. Bead-pull setup at SLAC with TIG welded cavity installed for measurements. (1) 1C-SW-A2.75-T2.0-TIG-Cu-Frascati-#1 cavity, (2) TM_{01} mode launcher, (3) nitrogen purge, and (4) fish-line pulley system for the bead pulling.

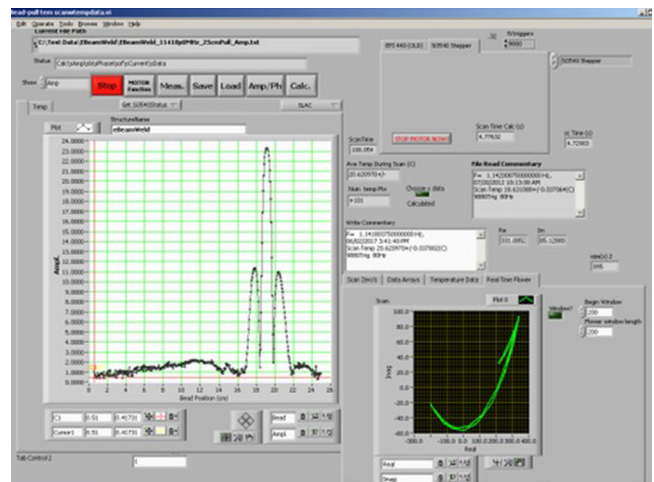


FIG. 5. LabView screen of the bead-pull control program showing the on-axis electric field profile of the TIG cavity measured with the non-resonant bead-pull technique.

SLAC and were both characterized with the non-resonant bead-pull technique [46]. For an example, we show the SLAC bead-pull setup used for the low-power rf measurements of the TIG welded structure in Fig. 4.

Figure 5 shows a LabView plot of the on-axis electric field in the TIG cavity measured with the bead-pull technique. The measured field profile is a good match with the simulated profile. The measured resonant frequency of the operating π mode of the nitrogen-filled cavity was 11.4186 GHz with a good quality factor of 9500.

IV. HIGH-POWER RF TESTS

A. Processing history

Two high-power experiments were performed; first with the EBW cavity (1C-SW-A2.75-T2.0-EBW-Cu-Frascati-#1) and second with the TIG welded cavity (1C-SW-A2.75-T2.0-TIG-Cu-Frascati-#1).

The rf power source was a SLAC 50 MW XL-4 klystron. In these experiments, the klystron was pulsed at 60 Hz producing a shaped rf pulse with a length up to 800 ns. The time evolution of the fields inside the cavity depends both on the rf properties of the cavity and the shape of the input rf pulse. We shaped the klystron pulse to create constant electric fields for a portion of the pulse [15,23]. The high-power conditioning process that we followed is well established and can be found in Refs. [13–16].

A schematic diagram of the test setup is given in Fig. 6. The klystron [(7) in Fig. 6] was connected to the structure (1) via a network of WR90 waveguides, with a 3 dB hybrid (5) used to reduce large reflections from the cavity to the klystron and back. The rf signals were sampled by two directional couplers (4) located before the mode launcher. The forward and reflected signals were both measured with a Keysight N1912A peak power meter (14) and downmixed (15) to be read by a fast digitizer (13). Two current monitors (3) on both sides of the cavity intercepted the field emitted electrons and were connected via coaxial cables to the same digitizer. A photo of the experimental setup with the TIG cavity installed inside the lead box is given in Fig. 7.

During the high-power tests of the EBW cavity, the high-gradient performance was not limited by the structure itself but likely by multipacting or arcing in the TM_{01} mode-launcher, which couples the rf power into the cavity. This arcing prevented us from increasing the power going into the cavity higher than 2 MW. Because of this limitation, we could not process the structure to its ultimate performance. However, below 2 MW, the breakdown signals were consistent with typical cavity breakdowns which enabled us to measure the breakdown rate in the EBW cavity.

Typically, we process structures of this type to much higher gradients and then measure the breakdown rate. At first, we suspected that the breakdowns at lower power were caused by the welded joints between the structure cells and the rf flanges. Nevertheless, during the post high-

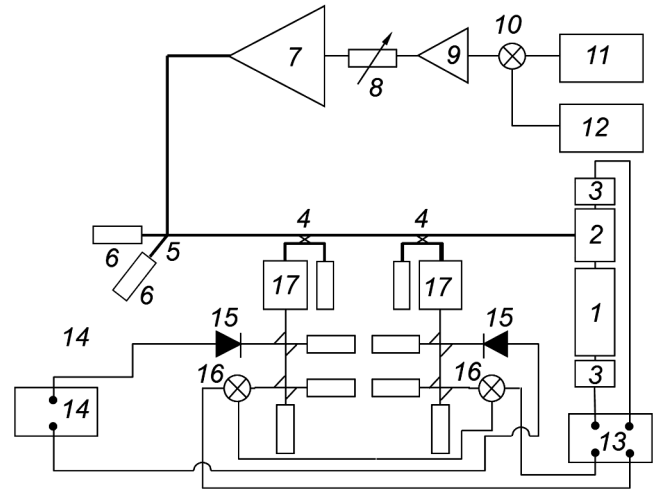


FIG. 6. Schematic diagram of the experimental setup: (1) 1C-SW-A2.75-T2.0-EBW-Cu-Frascati-#1 (first experiment) and 1C-SW-A2.75-T2.0-TIG-Cu-Frascati-#1 (second experiment), (2) TM_{01} mode launcher, (3) current monitors to measure field emission currents, (4) high-power directional couplers, (5) waveguide 3 dB hybrid, (6) high-power loads, (7) SLAC XL-4 X-band klystron, (8) variable attenuator, (9) traveling-wave tube amplifier, (10) mixer for klystron signal shaping, (11) 11 GHz signal generator, (12) arbitrary function generator for rf pulse shaping, (13) fast digitizer, (14) peak power meter, (15) probes of peak power meter, (16) phase-locked mixers with built-in local oscillators for rf signal measurements, and (17) low pass filters. Not numbered: cross guide directional couplers that couple signal between the low pass filter (17) and probes (15) and (16), and low power rf loads which are connected to high-power directional couplers (4) and cross guide directional couplers.

power test autopsy of the EBW cavity, we found no indication of unusual damage that could support that assumption and thus reduce cavity performance. The results of the cavity autopsy then led us to conclude that breakdowns happened somewhere else in the system. By

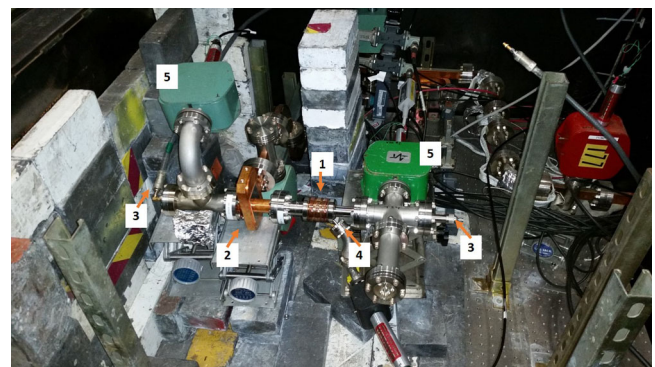


FIG. 7. The TIG structure installed inside the lead box. Experimental setup: (1) 1C-SW-A2.75-T2.0-TIG-Cu-Frascati-#1 cavity, (2) TM_{01} mode launcher, (3) coaxial cables to the current monitors, (4) port for secondary vacuum, and (5) high-vacuum ion pumps.

knowing this, we reprocessed the whole waveguide circuit in preparation for the TIG welded structure experiment. This reprocessing was done in two steps; first, we connected a high-power load in place of the cavity-mode launcher assembly and processed it up to 25 MW rf power and pulse length of 1.5 μ s, and second, we conditioned the TM_{01} mode launcher. In order to condition the mode launcher, we connected two mode launchers back-to-back and then to a high-power rf load. After that, we observed the same type of arcing behavior as we saw during the EBW structure testing. Then, we conditioned the back-to-back mode launchers up to 25 MW and 1.5 μ s pulse length.

At this point, we realized that arcing in the mode launcher was limiting the performance of the EBW cavity. This was supported by our observation that the behavior of the rf signals and the current monitor signals were consistent more with multipacting rather than vacuum breakdowns in the mode launcher.

B. Results

The breakdown rate was measured for the duration of 1–3 million pulses at a repetition rate of 60 Hz. During the measurements, the pulse shape was fixed and the gradient and the rate of breakdowns were relatively constant. We measured both trigger breakdown rates and total breakdown rates as discussed in Refs. [18–20]. The graphs below show the breakdown rate for the total number of breakdowns.

1. Breakdown performance of the EBW and TIG cavities

Here, we show the breakdown performance of the EBW and TIG welded hard copper structures compared with previously tested soft and hard copper structures of the same geometry. Note that the previously tested hard copper structures were joined by clamping. Figure 8 illustrates the results for a shaped pulse with a 150 ns flat part. The hard copper EBW structure demonstrated a gradient of about 90 MV/m with a breakdown rate of $10^{-3}/(\text{pulse meter})$. At the same breakdown rate, the TIG welded structure had a gradient of about 145 MV/m vs 190 MV/m for both soft and clamped hard copper structures. The slope of the breakdown rate vs gradient for both EBW and TIG is steeper than the previously tested soft and hard copper structures.

In Fig. 9, we show the results for a longer pulse (a shaped pulse with a 400 ns flat part). The hard copper EBW structure demonstrated a gradient of about 80 MV/m and the TIG structure demonstrated a gradient of about 130 MV/m, while both soft and clamped hard copper structures had a gradient of 160 MV/m with a breakdown rate of $10^{-3}/(\text{pulse meter})$. Also in this case, the slope of the breakdown rate vs the gradient for the welded structures is steeper than for the other two structures.

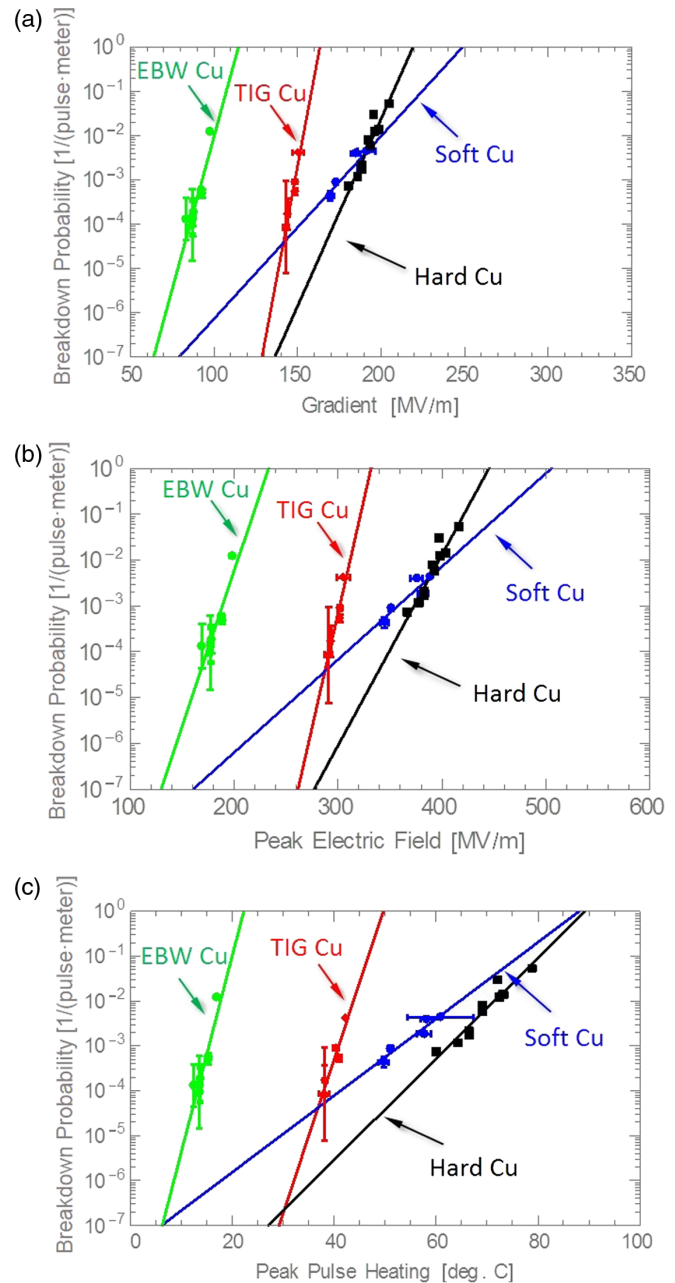


FIG. 8. Breakdown performance of EBW and TIG welded hard copper structures with soft and hard copper clamped structures, shaped pulse with 150 ns flat part. (a) breakdown rates vs accelerating gradient, (b) breakdown rates vs surface peak electric fields, and (c) breakdown rates vs peak pulse surface heating.

2. Breakdown probability dependence on pulse length

In this section, we illustrate breakdown probability dependence on pulse length. These measurements were done using our usual protocol which is described in Refs. [15,16]. We present the data below for rf pulses with different flat part lengths: 100, 150, 200, 400, and 600 ns.

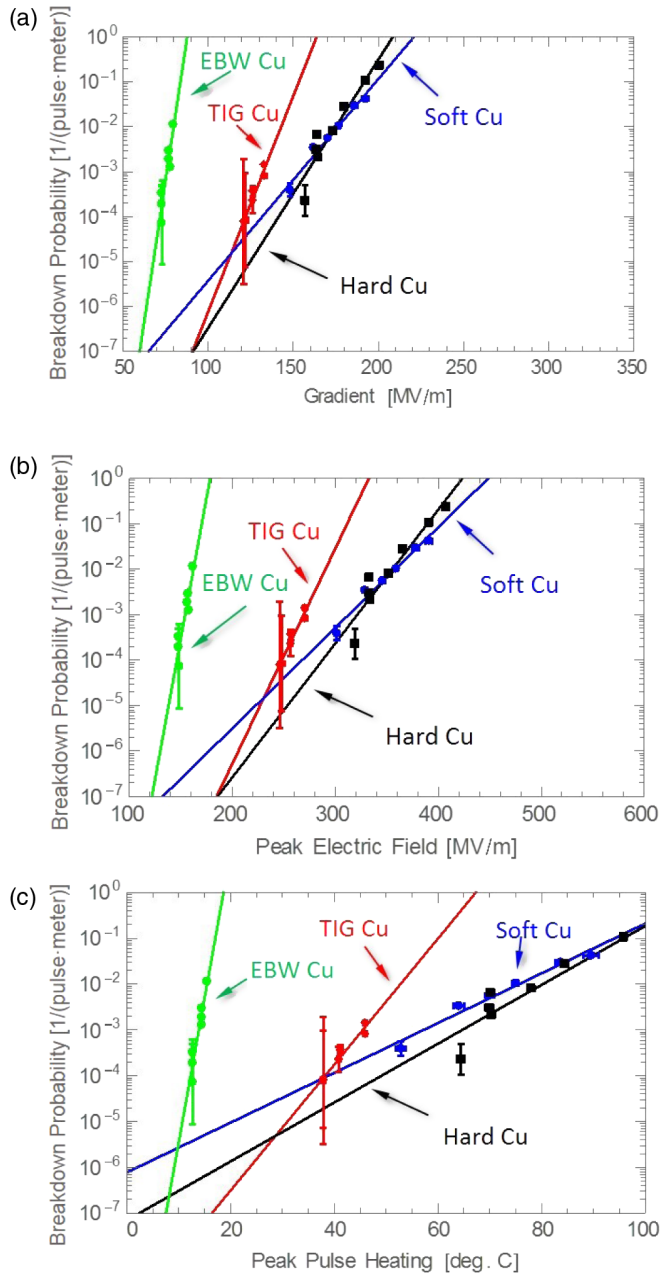


FIG. 9. Breakdown performance of EBW and TIG welded hard copper structures with soft and hard copper clamped structures, shaped pulse with 400 ns flat part. (a) breakdown rates vs accelerating gradient, (b) breakdown rates vs surface peak electric fields, and (c) breakdown rates vs peak pulse surface heating.

In Fig. 10, we show the data for the EBW structure. It seems that the peak pulse heating is a surprisingly good predictor of the breakdown rate. We know that the structure did not reach its ultimate performance, so these data are a snapshot of the metal's surface state on its way to further improvement, which we typically quickly bypass in our experiments. This may indicate that the surface stress induced by pulse surface heating plays a significant role

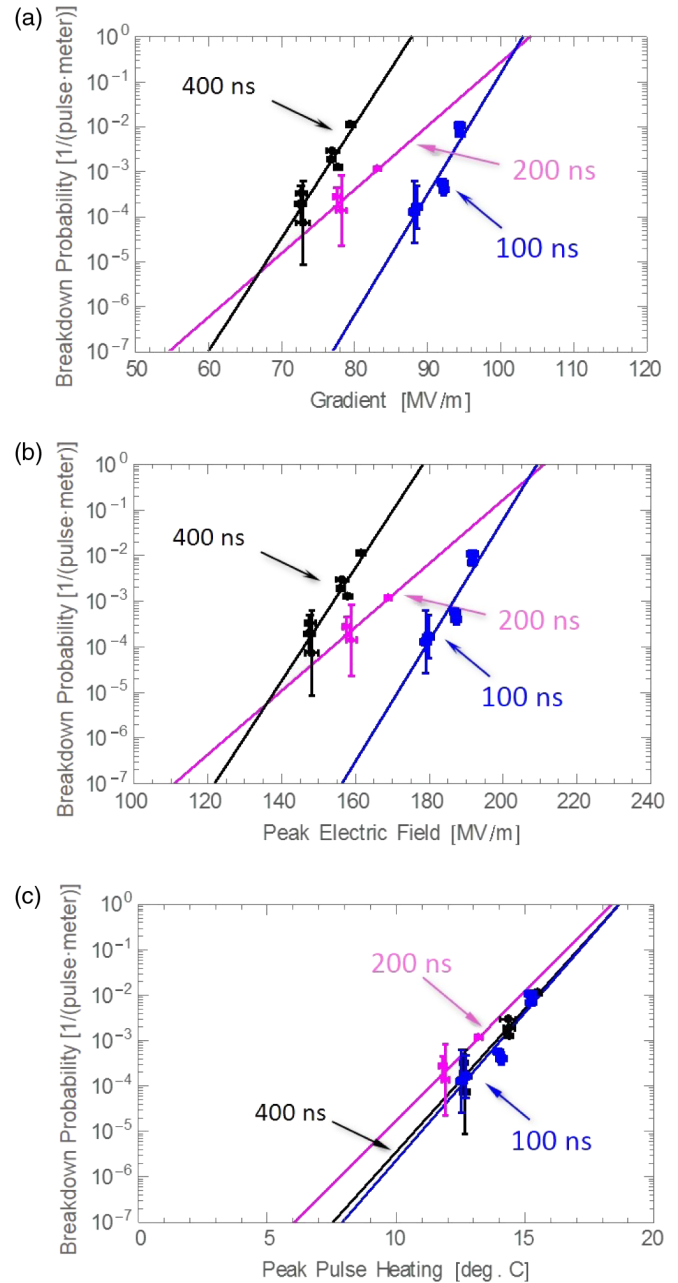


FIG. 10. The breakdown probability dependence on pulse length for the EBW hard copper structure, using shaped pulses with 100, 200, and 400 ns flat parts. (a) total breakdown rates vs accelerating gradient, (b) total breakdown rates vs peak surface electric fields, and (c) total breakdown rates vs peak pulse surface heating.

not only in ultimate breakdown performance but in the physics of the conditioning process.

In Fig. 11, we show the breakdown probability dependence on pulse length for the TIG welded structure. It seems that neither the peak surface fields nor peak pulse heating are good predictors of the breakdowns performance. It is likely that for short pulses, the breakdown rate depends more on the peak fields, and for longer pulses, it depends

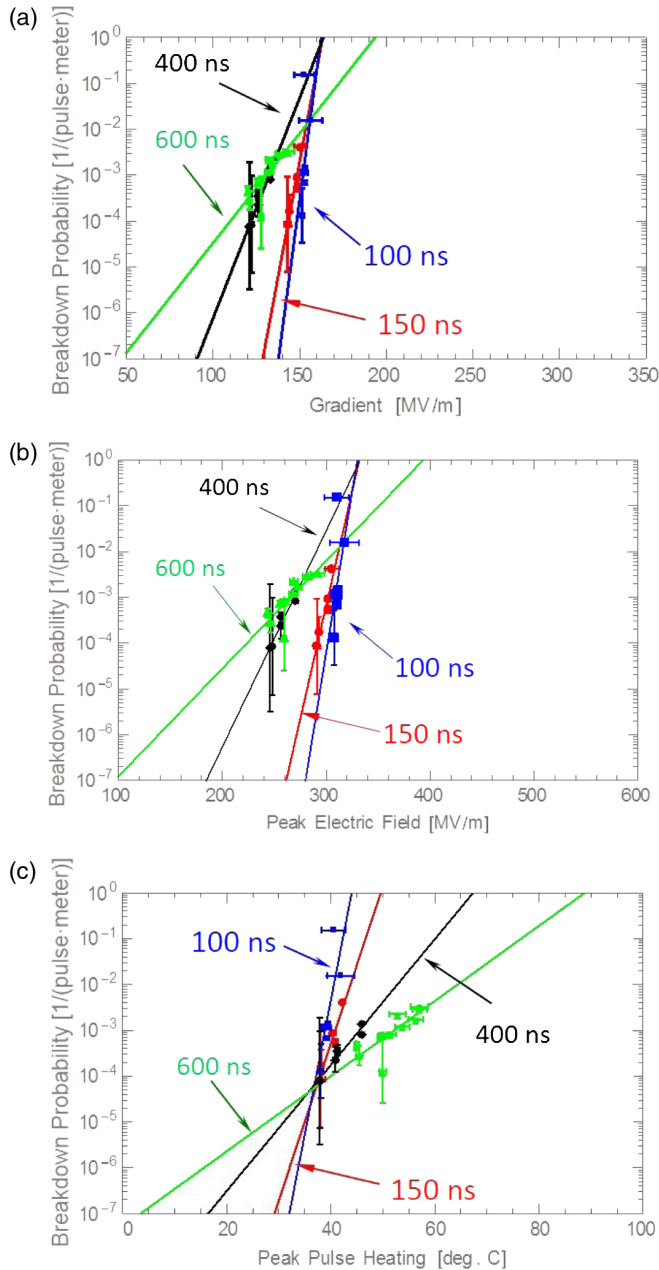


FIG. 11. The breakdown probability dependence on pulse length of TIG welded hard copper (1C-SW-A2.75-T2.0-TIG-Cu-Frascati-#1) structure, using shaped pulses with 100, 150, 400, and 600 ns flat parts. (a) breakdown rates vs accelerating gradient, (b) breakdown rates vs surface peak electric fields, and (c) breakdown rates vs peak pulse surface heating.

more on the peak pulse heating. We observed the same behavior in previously tested hard copper structures.

V. AUTOPSY RESULTS

We perform detailed autopsy on every tested structure. The autopsy is part of the validating process of our joining techniques. It shows whether or not the damage is associated specifically with these joining techniques. In this

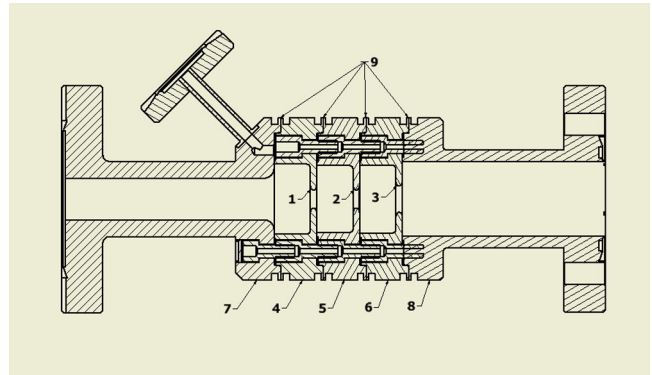


FIG. 12. Drawing of the TIG welded cavity, showing reference numbers and labels for the SEM analysis. (1), (2), and (3) are the irises of end, middle, and input cell, respectively; (4), (5), and (6) are the end, middle, and input cell, respectively; (7) and (8) are the adjoining drift sections; and (9) is the welding joints.

section, we discuss the results of the autopsies of the EBW and TIG welded structures. Both structures were cut at each of the outer joints and then unbolted. Various pieces were examined with a scanning electron microscope (SEM). For example, in Fig. 12, we illustrate the TIG cavity drawing which shows the numbering approach we used as reference for the autopsy analysis. In particular, we examined the following pieces with the SEM: the three cells (items 4, 5, and 6 in Fig. 12) and portions of the two adjoining drift sections (items 7 and 8). In addition, we examined the joint between the rf flange and a piece of the circular waveguide connected to it.

The autopsy results are divided into two sections. The first section is for the high-field areas, which are indicators of the surface quality and breakdown activity. The second

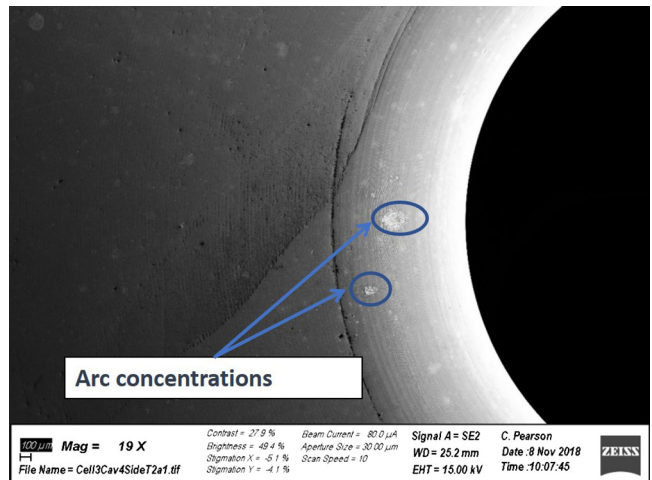


FIG. 13. Image of the middle cell side of iris 1 of the EBW structure. High-electric field areas have many small scattered arc pits. In addition, there are a few isolated locations that have concentrations of a very large number of arc pits, which are typically observed in these type of structures.

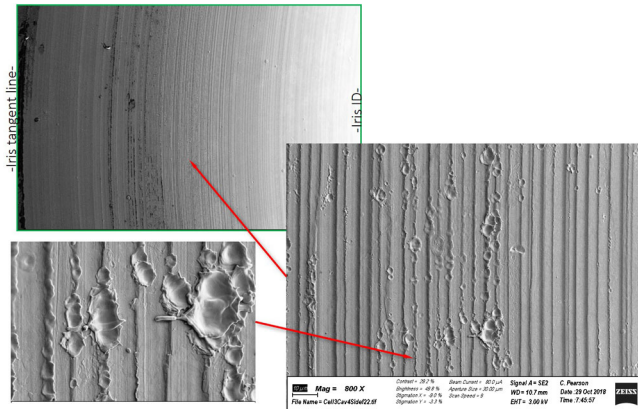


FIG. 14. EBW structure. Image of middle cell side of iris 1. Machining edges are obvious but there are no signs rf field-induced damage.

section is for the joints which show the quality of the electrical and mechanical contacts. The inspection of the joints is especially important for the validation of our method of cavity construction. Because the joints are high-current areas, the absence of rf-related damage shows that our construction method for both structures is valuable.

A. EBW cavity

1. High-field areas

The middle cell has evidence of the heaviest arcing, shown in Fig. 13. High-electric field areas have many small

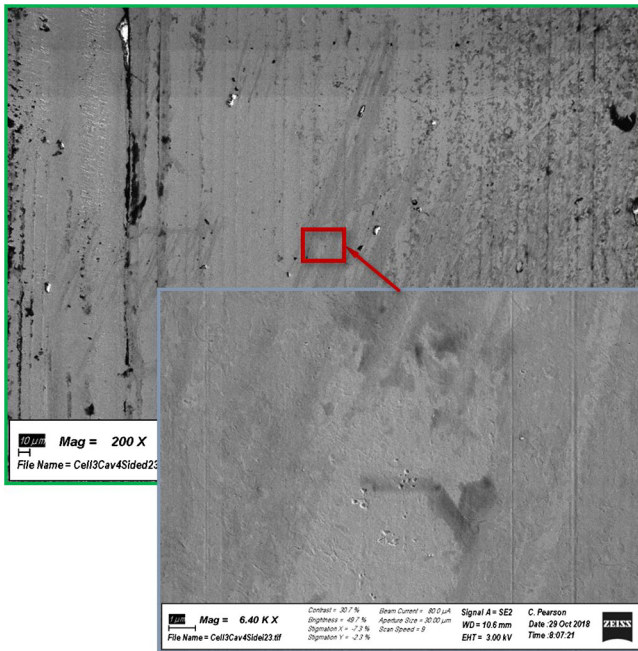


FIG. 15. EBW structure. Images of middle cell side of iris 1. High-magnetic field areas show no signs of pulse heating induced damage.

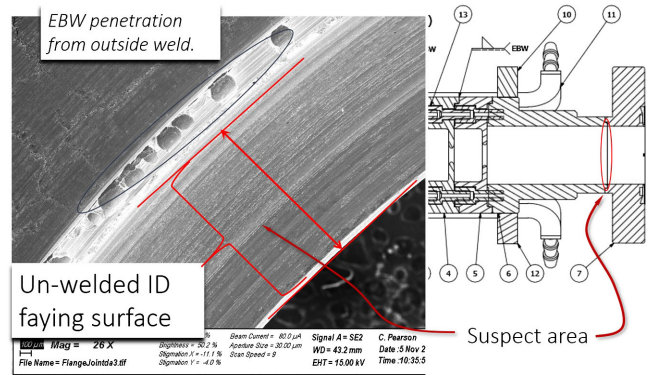


FIG. 16. EBW structure. Images of the waveguide to rf flange joint. No signs of rf-related damage.

scattered arc pits. In addition, there are a few isolated locations that have large concentrations of arc pits, which are typically observed in these type of structures. The dark line located at iris tangent point is carbon residue, likely due to contamination from the machining fluid. This carbon material appears to be incorporated into the melted copper. The dark spots are also carbon. Areas without arc concentrations appear pit free at low magnification, as shown in Fig. 14. However most of these areas are covered with small pits, often coincident with the sharp machining edges. We did not see magnetic field-induced damage in this area.

High-magnetic field areas have contamination but no signs of rf pulse heating damage (see Fig. 15).

2. Joints

The waveguide to the flange joint is not damaged by the rf fields, as seen in Fig. 16. However, the low beam voltage SEM image reveals a layer of carbon contamination on this

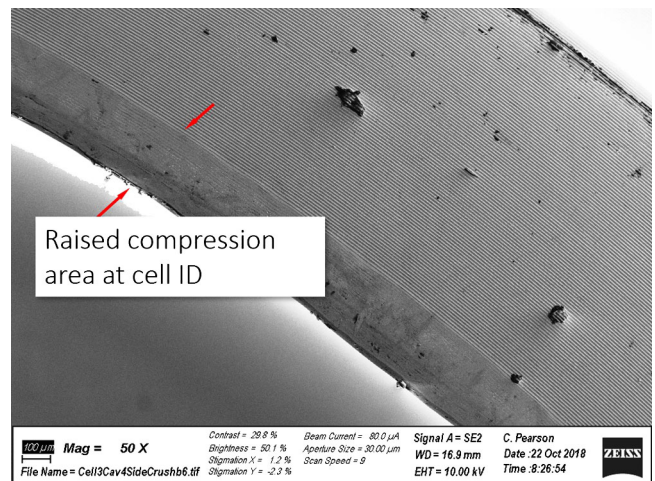


FIG. 17. EBW structure. Image of the inner seal area. No evidence of arcing or erosion related to high-rf currents.

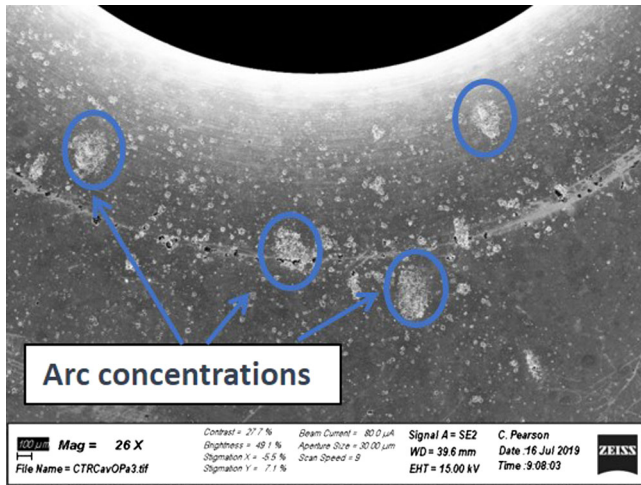


FIG. 18. TIG structure. Images of output side of middle cell. The high-electric field areas have many scattered small arc pits. In addition, there are a significant number of isolated locations that have high concentrations of arc pits, which is typical for these type of structures.

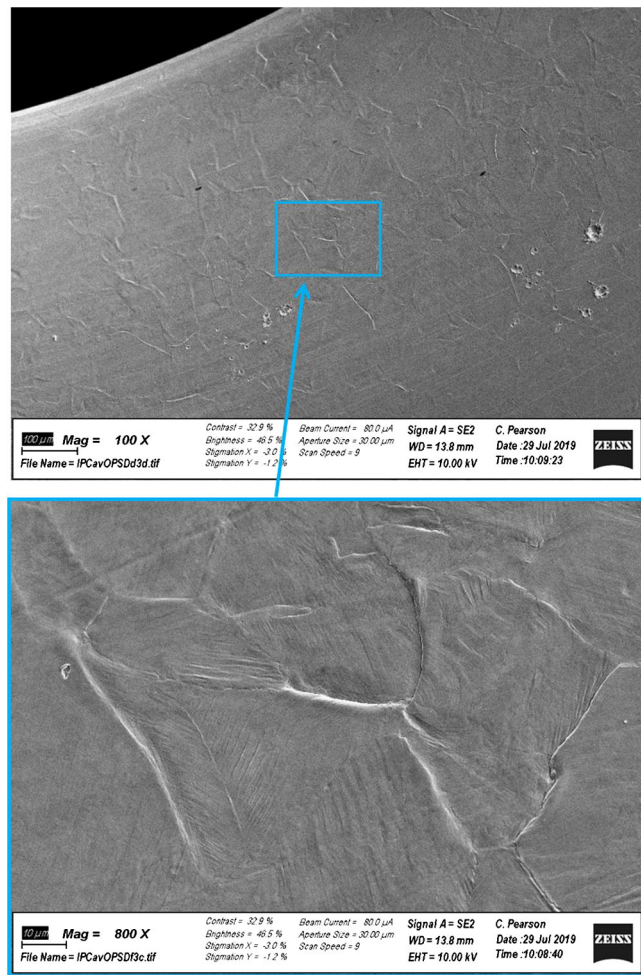


FIG. 19. TIG structure. Images of output side iris of input cell at a high-electric field area. This type of damage is typically associated with pulse surface heating in high-magnetic field areas.

surface. We initially suspected that a gap in this area was causing arcing and thus was limiting the cavity performance.

The compressed area of the cell-to-cell joints had no evidence of arcing or erosion related to high-rf currents, as shown in Fig. 17. This observation supports our assumption that the main cause limiting the cavity’s high-field performance was related to arcing in the TM_{01} mode launcher.

The performance of the cavity was limited by the mode launcher. However, we did not observe any rf-related damage neither in cell-to-cell joints nor in the rf flange-to-circular waveguide joint. This absence of joints damage validates our method of structure construction where we first clamped the cells with screws and then welded them. SEM images showed the cells were not chemically etched with our standard procedure developed for brazed structures. It is possible that the absence of the etching would have degraded the high-gradient performance of the cavity in comparison with our previous clamped structures, if the mode launcher was working well.

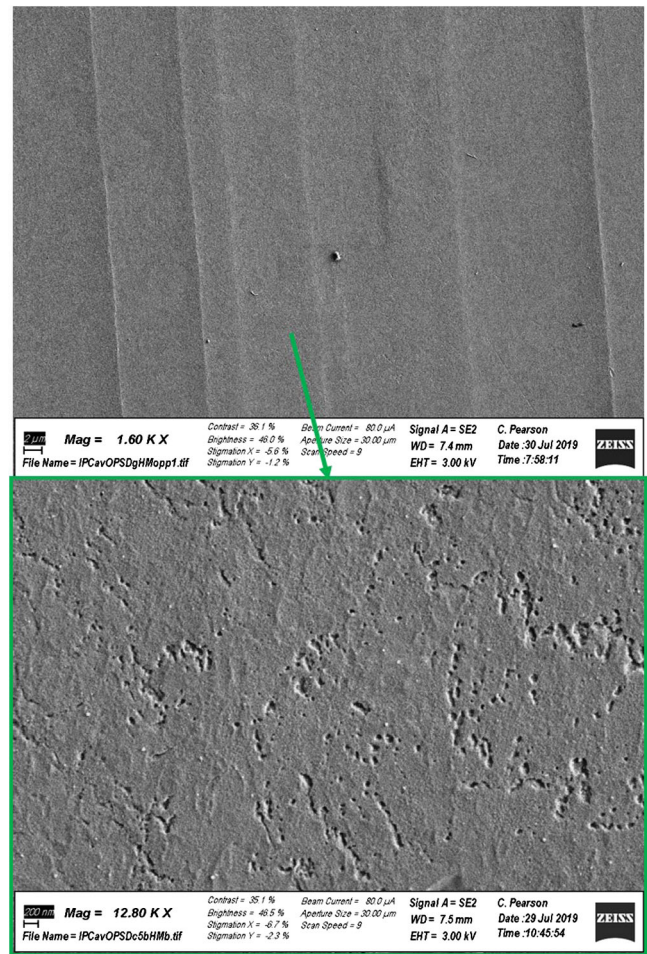


FIG. 20. TIG structure. Images of the output side outer surface of input cell. Top, high-magnetic fields areas; bottom, magnification in a region of these areas. The small pits are probably not rf-related.

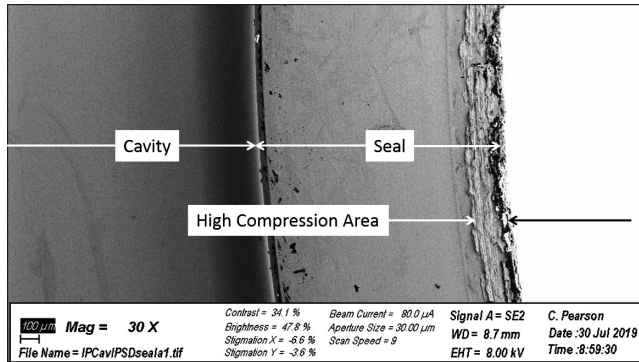


FIG. 21. TIG structure. Images of inner seal areas. No evidence of arcing was found.

B. TIG cavity

1. High-field areas

As expected, the middle cell has evidence of the heaviest arcing (see Fig. 18). The high-electric field areas have many scattered small arc pits. In addition, there are a significant number of isolated locations that have high concentrations of arc pits, which is typical for these type of structures. There are many areas of residual contamination, likely originating from machining operations.

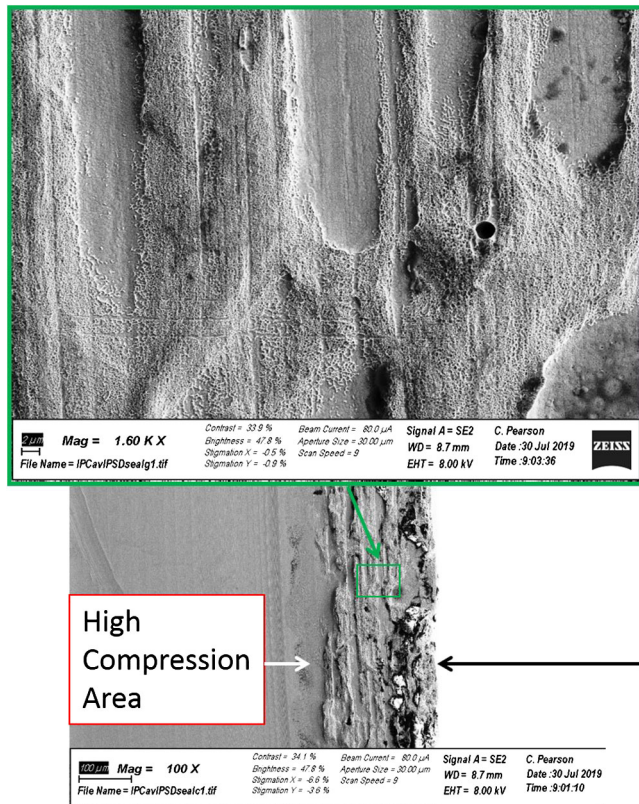


FIG. 22. TIG structure. Images of inner seal areas. The areas that appear raised and have a rougher texture are areas of incipient diffusion bonding.

As expected, the input cavity has much less arcing as seen in the SEM image of Fig. 19. There is apparent damage, which is typical for high-magnetic field areas and is usually associated with pulse surface heating. But in this case, it is in areas with high-electric fields. This damage manifests itself as slight topographic resurfacing which reveals the underlying grain structure caused by initial recrystallization due to the surface heating. Furthermore, the grain size, grain boundaries, and some indication of crystal orientation are evident in this image. The origin of this damage is not clear.

The high-magnetic field areas appear unaffected, which is typical for hard copper structures. As shown in Fig. 20, some pits are seen at high magnification (bottom), but they are probably not rf related.

2. Joints

All four inner compression seal areas were examined. No evidence of arcing was found as shown in Fig. 21. In Fig. 22, areas that appear raised and have a rougher texture are areas of incipient diffusion bonding. Overall, no features caused by high-power testing were detected.

VI. CONCLUSIONS

In the technological development of the construction methods of high-gradient accelerating structures, high-power testing is a critical step for the verification of their viability. Here, we present the outcome of this step, the results of the high-power rf tests of two X-band welded accelerating structures. This study is specifically about the validation of joining techniques; material processing will be the subject of further studies.

The EBW structure was successfully constructed and characterized at low power. During the high-power test, the input power was limited by possible multipacting inside the TM_{01} mode launcher to about 2 MW, so the structure did not reach its ultimate performance. However, the EBW cavity demonstrated an accelerating gradient of 90 MV/m at a breakdown rate of 10^{-3} /(pulse meter) using a shaped pulse with a 150 ns flat part. The steep slope of the measured breakdown rate for this structure vs the gradient is consistent with the steep slope of the hard-copper structures. It is not clear whether this steep slope is a property of the hard copper or a manifestation of an incomplete conditioning process. Nevertheless, the peak pulse heating is a surprisingly good predictor of the breakdown rate. We know that the structure did not reach its ultimate performance, so these data are a snapshot of the metal's surface state on its way to further improvement. In our previous experiments, we quickly bypassed this intermediate stage. These results may indicate that surface stress plays a significant role not only in the ultimate-high-field performance but also in the physics of the conditioning process. The autopsy showed no rf-related damage in the circular waveguide to the rf flange joint and the cell-to-cell

joints. This validates our method of structure construction and EBW as a part of it.

The TIG welded structure was successfully constructed and high power tested. The cavity performance showed about a 150 MV/m accelerating gradient at a breakdown rate of 10^{-3} /(pulse meter) using a shaped pulse with a 150 ns flat part. The slope of the breakdown rate vs the gradient for the TIG cavity is steeper than that of soft copper structures and close to that of CuAg structures. Neither gradient nor peak pulse surface heating are good predictors of the breakdown rate, which is not surprising for hard copper structures. The TIG welded structure did not reach the same performance as the hard copper structures we have tested before. A possible reason for that is the absence of chemical etching of high-gradient surfaces which we typically perform on high-gradient structures. Furthermore, we conjecture that the EBW performance would have been similar to that of TIG if there was no multipacting in the mode launcher.

We have designed a technique of cell clamping with special screws in order to build multicell structures. This technique is suitable for fabricating meter long structures. The autopsy performed after both tests have shown no rf-related damage in cell-to-cell joints. The results of this study represent an important step to validate our approach of building practical multicell structures made out of hard copper alloys.

ACKNOWLEDGMENTS

INFN/LNF work was supported by Committee V of INFN. SLAC work was supported by Department of Energy Contract No. DE-AC03-76SD00515. We would like to express our thanks to Fabio Cardelli for the preliminary low-power tests conducted at INFN-LNF. This work was made possible by the efforts of the SLAC's group of John Paul Eichner, Charles Yoneda, Andrew Haase, Chris Pearson, John Van Pelt, Brandon Weatherford, and the staff of the SLAC TID. We thank Sasha Dolgashev for proofreading the paper.

-
- [1] E. I. Simakov, V. A. Dolgashev, and S. G. Tantawi, Advances in high gradient normal conducting accelerator structures, *Nucl. Instrum. Methods Phys. Res., Sect. A* **907**, 221 (2018).
- [2] V. Dolgashev, Building and high power testing welded accelerating structures, in *Proceedings of the 12th International Workshop on Breakdown Science and High-Gradient Technology, HG2019, Chamonix, France* (CERN, Chamonix, France, 2019), <https://indico.cern.ch/event/766929/>.

- [3] V. Dolgashev, L. Faillace, B. Spataro, and R. Bonifazi, Innovative compact braze-free accelerating cavity, *J. Instrum.* **13**, P09017 (2018).
- [4] V. Dolgashev, L. Faillace, Y. Higashi, A. Marcelli, B. Spataro, and R. Bonifazi, Materials and technological processes for high-gradient accelerating structures: New results from mechanical tests of an innovative braze-free cavity, *J. Instrum.* **15**, P01029 (2020).
- [5] F. Wang, C. Adolphsen, and C. Nantista, Performance limiting effects in x-band accelerators, *Phys. Rev. ST Accel. Beams* **14**, 010401 (2011).
- [6] V. A. Dolgashev, Progress on high-gradient structures, in *AIP Conference Proceedings* (American Institute of Physics, New York, 2012), Vol. 1507, pp. 76–84.
- [7] V. Dolgashev, S. Tantawi, Y. Higashi, and B. Spataro, Geometric dependence of radio-frequency breakdown in normal conducting accelerating structures, *Appl. Phys. Lett.* **97**, 171501 (2010).
- [8] V. A. Dolgashev and S. G. Tantawi, Effect of rf parameters on breakdown limits in high-vacuum X-band structures, *AIP Conf. Proc.* **691**, 151 (2003).
- [9] V. A. Dolgashev, High magnetic fields in couplers of X-band accelerating structures, in *Proceedings of the 2003 Particle Accelerator Conference* (IEEE, New York, 2003), Vol. 2, pp. 1267–1269.
- [10] V. A. Dolgashev and S. G. Tantawi, Simulations of currents in X-band accelerator structures using 2D and 3D particle-in-cell code, in *Proceedings of the 19th Particle Accelerator Conference, Chicago, IL, 2001* (IEEE, Piscataway, 2001).
- [11] V. A. Dolgashev and S. G. Tantawi, Rf breakdown in X-band waveguides, in *Proceedings of the 8th European Particle Accelerator Conference, Paris, 2002* (EPS-IGA and CERN, Geneva, 2002), p. 2139.
- [12] V. A. Dolgashev, High gradient, X-band and above, metallic rf structures, in *Proceedings of the 2nd European Advanced Accelerator Concepts Workshop, 2015 Workshop, EAAC 2015* (2015).
- [13] V. Dolgashev, B. Spataro, A. Yeremian, Y. Higashi, and S. Tantawi, Status of high power tests of normal conducting single-cell standing wave structures, *Conf. Proc.* **100523**, THPEA060 (2010).
- [14] L. Laurent, S. Tantawi, V. Dolgashev, C. Nantista, Y. Higashi, M. Aicheler, S. Heikkinen, and W. Wuensch, Experimental study of rf pulsed heating, *Phys. Rev. ST Accel. Beams* **14**, 041001 (2011).
- [15] A. Cahill, J. Rosenzweig, V. A. Dolgashev, S. G. Tantawi, and S. Weathersby, High gradient experiments with X-band cryogenic copper accelerating cavities, *Phys. Rev. ST Accel. Beams* **21**, 102002 (2018).
- [16] A. Cahill, J. Rosenzweig, V. Dolgashev, Z. Li, S. Tantawi, and S. Weathersby, RF losses in a high gradient cryogenic copper cavity, *Phys. Rev. ST Accel. Beams* **21**, 061301 (2018).
- [17] C. Nantista, S. Tantawi, and V. Dolgashev, Low-field accelerator structure couplers and design techniques, *Phys. Rev. ST Accel. Beams* **7**, 072001 (2004).

- [18] B. J. Munroe, A. M. Cook, M. A. Shapiro, R. J. Temkin, V. A. Dolgashev, L. L. Laurent, J. R. Lewandowski, A. D. Yeremian, S. G. Tantawi, and R. A. Marsh, High power breakdown testing of a photonic band-gap accelerator structure with elliptical rods, *Phys. Rev. ST Accel. Beams* **16**, 012005 (2013).
- [19] R. A. Marsh, M. A. Shapiro, R. J. Temkin, V. A. Dolgashev, L. L. Laurent, J. R. Lewandowski, A. D. Yeremian, and S. G. Tantawi, X-band photonic band-gap accelerator structure breakdown experiment, *Phys. Rev. ST Accel. Beams* **14**, 021301 (2011).
- [20] V. Dolgashev, G. Gatti, Y. Higashi, O. Leonardi, J. Lewandowski, A. Marcelli, J. Rosenzweig, B. Spataro, S. Tantawi, and D. Yeremian, High power tests of an electroforming cavity operating at 11.424 GHz, *J. Instrum.* **11**, P03010 (2016).
- [21] J. Wang, T. Higo, J. Van Pelt, B. Gudkov, C. Yoneda, J. Lewandowski, G. Riddone, and T. Takatomi, Fabrication technologies of the high gradient accelerator structures at 100 MV/m range, *Conf. Proc.* **100523**, THPEA064 (2010).
- [22] T. Higo, Y. Higashi, S. Matsumoto, K. Yokoyama, C. Adolphsen, V. Dolgashev, A. Jensen, L. Laurent, S. Tantawi, F. Wang *et al.*, Advances in X-band TW Accelerator Structures Operating in the 100 MV/m Regime, *Conf. Proc.* **C100523**, THPEA013 (2010); SLAC National Accelerator Lab., Menlo Park, CA, USA, SLAC-PUB-15150, 2012.
- [23] R. A. Marsh, M. A. Shapiro, R. J. Temkin, V. A. Dolgashev, L. L. Laurent, J. R. Lewandowski, A. D. Yeremian, and S. G. Tantawi, X-band photonic band-gap accelerator structure breakdown experiment, *Phys. Rev. ST Accel. Beams* **14**, 021301 (2011).
- [24] M. Ferrario and D. Alesini, M. P. Anania, M. Artioli, A. Bacci, S. Bartocci, R. Bedogni, M. Bellaveglia, A. Biagioni, F. Bisesto *et al.*, EuPRAXIA@ SPARC_LAB Design study towards a compact FEL facility at LNF, *Nucl. Instrum. Methods Phys. Res., Sect. A* **909**, 134, 2018.
- [25] P. Emma, R. Akre, J. Arthur, R. Bionta, C. Bostedt, J. Bozek, A. Brachmann, P. Bucksbaum, R. Coffee, F.-J. Decker *et al.*, First lasing and operation of an angstrom-wavelength free-electron laser, *Nat. Photonics* **4**, 641 (2010).
- [26] A. Degiovanni, W. Wuensch, and J. G. Navarro, Comparison of the conditioning of high gradient accelerating structures, *Phys. Rev. ST Accel. Beams* **19**, 032001 (2016).
- [27] A. Degiovanni, J. Kovermann, W. Farabolini, R. Wegner, S. Doebert, B. Woolley, I. Syratchev, W. Wuensch, A. Solodko, E. Montessinos *et al.*, High-gradient test results from a CLIC prototype accelerating structure: TD26CC, in *Proceedings of the 5th international Conference IPAC2014, Dresden, Germany* (JACoW Publishing, 2014).
- [28] W. Wuensch, Advances in the understanding of the physical processes of vacuum breakdown, Technical Reports No. CERN-OPEN-2014-028, No. CLIC-NOTE-1025, 2013.
- [29] T. Argyropoulos, N. Catalan-Lasheras, A. Grudiev, G. Mcmonagle, E. Rodriguez-Castro, I. Syrachev, R. Wegner, B. Woolley, W. Wuensch, H. Zha, and V. Dolgashev, Design, fabrication, and high-gradient testing of an X-band, traveling-wave accelerating structure milled from copper halves, *Phys. Rev. Accel. Beams* **21**, 061001 (2018).
- [30] J. Shao, C. Jing, S. Antipov, M. Conde, W. Gai, Q. Gao, G. Ha, W. Liu, N. Neveu, J. Power *et al.*, Recent two-beam acceleration activities at argonne wake field accelerator facility, *Proc. IPAC* **17**, 3305 (2017).
- [31] W. Brown, S. Korbly, K. Kreisler, I. Mastovsky, and R. Temkin, Low emittance electron beam formation with a 17 ghz rf gun, *Phys. Rev. ST Accel. Beams* **4**, 083501 (2001).
- [32] S. Matsumoto, W. Wuensch, G. Riddone, T. Higo, and I. Syratchev, High power evaluation of X-band high power loads, in *Proceedings of Linear Accelerator Conference LINAC2010, Tsukuba, Japan* (2010).
- [33] J. Shi, X. Wu, C. Jing, Y. Yang, H. Zha, Q. Gao, W. Gai, and H. Chen, Development of an x-band metallic power extractor for the argonne wakefield accelerator, in *Proceedings of the 4th International Particle Accelerator Conference (IPAC13)* (JACoW, 2013), pp. 2771–2773.
- [34] B. J. Munroe, A. M. Cook, M. A. Shapiro, R. J. Temkin, V. A. Dolgashev, L. L. Laurent, J. R. Lewandowski, A. D. Yeremian, S. G. Tantawi, and R. A. Marsh, High power breakdown testing of a photonic band-gap accelerator structure with elliptical rods, *Phys. Rev. ST Accel. Beams* **16**, 012005 (2013).
- [35] J. Giner Navarro, Breakdown studies for high-gradient rf warm technology in: CLIC and hadron therapy linacs, Ph.D. thesis Dissertation, Universitat de Valencia, Departamento de Fisica Atomica Molecular Y Nuclear, 2016, <https://dialnet.unirioja.es/servlet/dctes?codigo=180608>.
- [36] N. Catalan, CERN Testing program: Plans and schedule, in *Proceedings of the International Workshop on Breakdown Science and High Gradient Accelerator Technology (HG2016)* (Argonne National Laboratory, Lemont, 2016).
- [37] W. Wuensch, Status and objectives of the CLIC X-band and high-gradient activity, in *International Workshop on Breakdown Science and High Gradient Technology in Tsukuba, Japan* (CERN, Tsukuba, 2012).
- [38] T. Higo, Progress of X-Band Accelerating Structures, in *Proceedings of the 25th International Linear Accelerator Conference, LINAC2010: Tsukuba, Japan, 2010* (JACoW, 2011), p. FR104.
- [39] A. Grudiev, S. Calatroni, and W. Wuensch, New local field quantity describing the high gradient limit of accelerating structures, *Phys. Rev. ST Accel. Beams* **12**, 102001 (2009).
- [40] V. A. Dolgashev, S. G. Tantawi, C. D. Nantista, Y. Higashi, and T. Higo, Rf breakdown in normal conducting single-cell structures, in *Proceedings of the 2005 Particle Accelerator Conference* (JACoW, 2005), pp. 595–599.
- [41] H. Zha, V. Dolgashev, and A. Grudiev, RF design of the CLIC structure prototype optimized for manufacturing from two halves, in *Proceedings of the 6th International Particle Accelerator Conference, IPAC 2015, Richmond, Virginia, USA, 2015* (2015).
- [42] M. Dal Forno, V. Dolgashev, G. Bowden, C. Clarke, M. Hogan, D. McCormick, A. Novokhatski, B. Spataro,

- S. Weathersby, and S. G. Tantawi, Rf breakdown tests of mm-wave metallic accelerating structures, *Phys. Rev. ST Accel. Beams* **19**, 011301 (2016).
- [43] M. Dal Forno, V. Dolgashev, G. Bowden, C. Clarke, M. Hogan, D. McCormick, A. Novokhatski, B. O'Shea, B. Spataro, S. Weathersby *et al.*, High gradient tests of metallic mm-wave accelerating structures, *Nucl. Instrum. Methods Phys. Res., Sect. A* **864**, 12 (2017).
<https://www.ansys.com/products/electronics/ansys-hfss>.
- [44] <https://www.ansys.com/products/electronics/ansys-hfss>.
- [45] R. Bonifazi, Comeb srl, <https://www.comeb.it>.
- [46] C.W. Steele, A nonresonant perturbation theory, *IEEE Trans. Microwave Theory Tech.* **14**, 70 (1966).